

Reaction mechanism of quasi-free knockout processes in exotic RI beam era

Kazuki Yoshida¹ and Junki Tanaka²

¹*Advanced Science Research Center, Japan Atomic Energy Agency, Tokai, Ibaraki 319-1195, Japan*

²*Research Center for Nuclear Physics, Ibaraki, Osaka 567-0047, Japan*

.....
 The quasi-free nucleon knockout reaction has been revealed the single-particle nature of nuclei. Thanks to the advances in experimental techniques and reaction theory, various new aspects of nuclei are being revealed by knockout reactions. In this article, we review the basic concept of the quasi-free knockout reaction, and recent achievements in the SEASTAR project using the MINOS system. We also present our new findings on the low-energy nucleon knockout reaction and the α knockout reaction. The combination of the (microscopic) structure theory, reaction theory and experiments will be the key to a complete understanding of the α formation and its universality in the coming decades. Noble clusters, e.g., d , t , ${}^3\text{He}$, etc. are in the scope of the ONOKORO project. The implementation of the two (and more) nucleon correlation in the reaction theory is essential to connect the properties of such clusters and the reaction observables. A new framework, CDCCIA, is introduced for this purpose, which will also be applicable to the two-nucleon knockout reactions, e.g., $(p, 3p)$, $(p, 2pn)$, and $(p, p2n)$.

1 Introduction

A correct description of the quasi-free knockout reaction mechanism leads from experimental observables to information about the internal structure of atomic nuclei. Such research has been conducted since the middle of the 20th century [1–4], and progress has been made in understanding the structure of stable nuclei. Physical quantities observed in proton-induced knockout reactions targeting stable nuclei provided the excitation energy distribution of residual nuclei, the occupancy of nucleons in single particle orbits, their momentum distributions, and so on. Recent research has indicated that the reaction cross sections of the α cluster knockout reaction are roughly proportional to the amount of α cluster formation on the nuclear surface, which isotopic dependence of the reaction cross sections showed a good agreement with a theoretical prediction [5–10]. Systematic cluster knockout reaction experiments are being performed to investigate the various clusters formed on the nuclear surface. On the other hand, in research using RI beams, experimental techniques using inverse kinematics have improved, and many research results using quasi-free scattering of unstable nuclei have been reported in the past decades, leading to progress in understanding unstable nuclear structures.

Inverse kinematics experiments using RI beams have several advantages: In proton-induced knockout reactions, a heavy ion beam is incident on a hydrogen target [11]. The emitted recoil protons have relatively high energy and are possible to measure. Because the proton is at rest in the initial state, the energy of the proton in the final state is nothing but the energy transfer that characterizes the reaction kinematics. There are various types of knockout particles, including nucleons, such as protons and neutrons, and light ions, which are cluster particles. Measurement of these protons and knocked-out particles will complement the missing mass. In addition, the momentum distribution of the residual nucleus reflects the inter-nuclear momentum distribution of the knocked-out particle, and since it travels straight with almost the same energy as the incoming beam in the laboratory frame, detailed analysis with spectrometers is possible. Reaction channels in which the final state decomposes into many particles can also be measured because the emitted particles are ejected forward with energy comparable to that of the incoming beams again, and these measurements give an invariant mass. Due to these unique advantages of inverse kinematics, a wide variety of physical quantities can be measured, and the opportunities for more detailed reaction and structural research in RI beam research are increasing.

In theory, the knockout reaction is solved in the center-of-mass frame in practice. The laboratory frame, either the forward or the inverse kinematics, and the center-of-mass frame are connected by the Lorentz transformation in principle. However, the observables may be

different depending on the kinematics, in general kinematically more exclusive cross sections such as the triple-differential cross section are measured in the forward kinematics, while the 1D longitudinal or transverse momentum distribution is usually discussed in the inverse kinematics as in the SEASTAR. Since the knockout reaction is the three-body reaction, its kinematics and observables in the forward and the inverse kinematics, and their relation are rather complicated, as overviewed in a recent article [12]. It should be noted here that recently the triple-differential cross section of $(p, p\alpha)$ reaction has been measured and analyzed [13]. Also, the quadruple differential cross section is recently proposed [14], which brings us natural correspondence between the particle motion inside a nucleus and the shape of the cross section.

From the viewpoint of the reaction mechanism, when the incident nuclear spallation reaction first initiated the RI beam era, the reaction mechanism was simplified, and the momentum distributions are described by the Goldhaber model [15] to the zeroth approximation. Since then, the production cross section of incident nuclear spallation reactions has been systematically studied from a macroscopic perspective, and an empirical code for calculating the production cross section using the Glauber model, evaporation model, and intranuclear cascade model [16–22] has been developed. This method has been applied to systematic studies of reaction cross sections and transmutation of nuclear fuel waste. This framework treats knockout reactions as the classical multiple collisions of nucleons. On the other hand, in nuclear structural research, we aim to elucidate reaction mechanisms from a more microscopic perspective, focusing on reaction channels. Inclusive measurements have become popular with the rise of measurement instruments such as MINOS that support inverse kinematics using RI beams, and accurate theoretical descriptions of reaction mechanisms are essential to explain experimental data. It should be also noted here that only a nucleon and an α can be regarded as an inert, simple one particle in describing the knockout reactions. Novel clusters such as deuteron, triton, and ^3He , etc., have to be treated as fragile particles, and the coupling and transition between their ground state and excited and continuum states during the reaction.

In this paper, we review the knockout reaction mechanism from a microscopic perspective. Section 2 explains the knockout reaction theory. Next, In Sec. 3 the nucleon knockout reactions are reviewed. We will explain the momentum distribution and its asymmetry obtained in experiments using the RI beam and the MINOS device, using the reaction mechanism introduced in Sec. 2. In Sec. 4, recent research for probing the α particle formation in nuclei ranging from light to heavy mass regions are introduced. The surface sensitivity of the α knockout reaction allows us to deduce the reduced α decay width from the α knockout cross

section, independently from the Coulomb barrier penetration process of the α decay. Furthermore, in Sec. 5, we will go beyond the standard nucleon and α knockout reactions and discuss two-proton knockout reactions and deuteron knockout reactions. To quantitatively connect the information of the deuteron-like pn pair and correlated pp pair formed in a nucleus and knockout cross section of them, it is essential to describe the complex reaction mechanism and theoretical progress has to be made.

2 Quasi-free NN scattering inside nucleus

The proton-induced nucleon knockout reaction, (p, pN) , is described as a three-body reaction of the incident proton, struck nucleon N , and the core (residual) nucleus B. The target nucleus A is regarded as a bound state of N and B. The incident proton, outgoing proton, and struck N are labeled as particles 0, 1, and 2, respectively. The coordinates between these particles are defined as shown in Fig. 1.

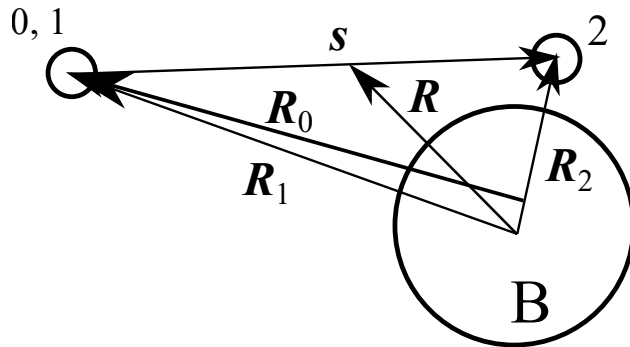


Fig. 1 Coordinate and label for the particles.

2.1 Impulse approximation

In this section, the essence of the knockout reaction and the triple differential cross section, the quadruple differential cross section, and the momentum distributions are introduced based on the distorted-wave impulse approximation (DWIA). Note that, although the equations are based on the DWIA, those quantities are essential ones in describing the knockout reaction cross sections regardless of the theoretical framework employed. Based on the multiple scattering theory [23–25], the scattering of a nucleon from a nucleus can be described in terms of the multiple scattering between the incident nucleon and the nucleons in the target. From this perspective, (p, pN) reaction can be regarded as an extreme case in which only a single nucleon inside a nucleus is involved in the reaction. First of all, we

recall the impulse approximation as a high energy approximation on the NN collision inside a nucleus [26], which supports our naive picture of the knockout reaction. In terms of the bare NN interaction v_{01} and the Green's operator G , the effective interaction τ_{01} of the NN collision inside a nucleus A is given by

$$\tau_{01} = v_{01} (1 + G\tau_{01}), \quad (1)$$

$$G = (E - H + i\varepsilon)^{-1}. \quad (2)$$

Here, H is not the free Hamiltonian but it contains the interaction between the bound nucleon and B, V_{1B} . In the nucleus A rest frame, G can be written as

$$G = (E_A - T_0 - T_1 - T_B - V_{1B} + i\varepsilon)^{-1}, \quad (3)$$

where E_A is the total energy in the A rest frame, T_0 , T_1 , and T_B are the kinetic energy operator of particle 0, 1, and B, respectively. First, the impulse approximation assumes that V_{1B} is negligible compared to E_A when the incident proton has high kinetic energy. In addition, since $T_B \approx T_1/(A-1)$ in the A rest frame, T_B can be neglected when A is large. Thus, G can be approximated as

$$G \approx G_0 = (E_A - T_0 - T_1 + i\varepsilon)^{-1}, \quad (4)$$

which is the free Green's operator of the NN scattering in the free space. This approximation results in the free NN t -matrix as

$$\tau_{01} \approx t_{01} = v_{01} (1 + G_0 t_{01}). \quad (5)$$

2.2 Distorted wave impulse approximation

Based on the impulse approximation, the DWIA framework [3, 4, 27] employs the NN effective interaction as a transition interaction of the (p, pN) reaction. Its transition matrix is given by

$$T = \langle \chi_1 \chi_2 \Phi_1 \Phi_2 \Phi_B | t_{01} | \chi_0 \Phi_0 \Phi_A \rangle. \quad (6)$$

χ_0 , χ_1 , and χ_2 are the distorted waves between particles 0 and A, 1 and B, 2 and B, respectively. The internal wave function of particles ($i = 0, 1, 2, A, B$) are denoted by Φ_i . Note that the indices for the spin, isospin, etc., are omitted from Eq. (6) for simplicity. If the particle i is a nucleon, Φ_i only represents its particle number, spin, and isospin. In the plane-wave limit (PW), Eq. (6) is reduced to a product of the NN t -matrix element and the overlap wave function as

$$T \xrightarrow{\text{PW}} \langle \boldsymbol{\kappa}' | t_{01} | \boldsymbol{\kappa} \rangle \tilde{\varphi}_2(\mathbf{k}_2), \quad (7)$$

where $\boldsymbol{\kappa}$ ($\boldsymbol{\kappa}'$) is the relative momentum between particle 0 and 1 in the initial (final) state and \boldsymbol{k}_2 is the momentum of particle 2 inside the target nucleus A, which can be approximately determined by the knockout reaction kinematics. The overlap function φ_2 in is defined as

$$\varphi_2 = \langle [\Phi_2 \otimes \Phi_B] | \Phi_A \rangle \quad (8)$$

and $\tilde{\varphi}_2$ is that in the momentum space. The triple differential cross section, which is the most kinematically exclusive cross section of the knockout reaction, is given by

$$\frac{d^3\sigma^X}{dE_1 d\Omega_1^X d\Omega_2^X} = \mathcal{J}_{XG} F_{\text{kin}}^X \frac{(2\pi)^4}{\hbar v_\alpha} \frac{1}{(2s+1)(2j+1)} \sum_{\text{spins}} |T|^2. \quad (9)$$

Here, E_i is the total energy of particle i and Ω_i is the solid angle of the emitted direction of particle i . \mathcal{J}_{XG} is the Jacobian from the center-of-mass frame to an arbitrary X-frame

$$\mathcal{J}_{XG} = \frac{E_1 E_2 E_B}{E_1^X E_2^X E_B^X}, \quad (10)$$

and F_{kin}^X is the phase volume. v_α is the Lorentz invariant velocity of the incident particle. The spin of the incident particle and the total angular momentum of the struck particle inside the target are denoted by s and j , respectively. The summation over all the spin degrees of freedom is taken in Eq. (10).

It is seen from Eqs. (7) and (10) that in the plane-wave limit, the knockout cross section is proportional to $|T|^2$ and it shows the momentum distribution of the struck particle inside the nucleus A. In reality, the scattering waves are not the plane waves but the distorted waves under the optical potentials. Thus the momentum distribution of the knockout reaction is also distorted. See [3, 4, 14, 27] for the detailed derivation of DWIA equations for the knockout reaction.

3 Nucleon knockout reaction

3.1 Momentum distribution and the single-particle orbit

As discussed in Sec. 2.2, the momentum distribution of the knockout cross section tells us the single-particle orbit of the struck particle, since the width of the momentum distribution becomes wider as the orbital angular momentum becomes larger. A typical example is shown in Ref. [28] and Fig. 2. The longitudinal momentum distribution of $^{54}\text{Ca}(p, pn)^{53}\text{Ca}$ reaction leaving the ^{53}Ca residue in the ground-state, 2220 and 1738 keV excited states are shown. The ordering of the neutron orbitals in ^{54}Ca is expected to be different from a traditional one due to the shell evolution driven by the lack of the tensor force between the neutron $1f_{5/2}$

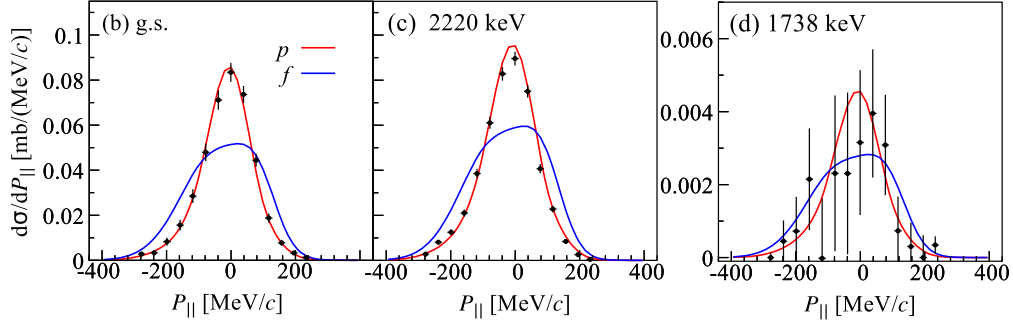


Fig. 2 Longitudinal momentum distribution of $^{54}\text{Ca}(p, pn)^{53}\text{Ca}$ reaction. (b) The ^{54}Ca is in the ground state, (c) 2220 keV state (d) 1738 keV state. Reprinted figure with permission from [28] Copyright 2024 by the American Physical Society.

and proton $1f_{7/2}$ orbitals in such neutron-rich nuclei [29, 30]. The comparison between the data and the DWIA curves strongly suggests that the valence neutron is in the p -wave, which supports the shell evolution in the pf shell in the neutron-rich nuclei and the emergence of $N = 34$ shell closure.

3.2 Knockout reaction at low energy and the asymmetry of the momentum distribution

It has been known that the longitudinal momentum distribution (LMD) of the nucleon removal reaction is asymmetric. See Figs. 2 and 3 of Ref. [31] for example. In contrast, it has been also known that the LMD of the neutron halo removal reaction is almost symmetric (See Fig. 3 of Ref. [32]). The asymmetry of LMD has been theoretically discussed based on the DWIA framework [33]. The steep cut at the high momentum side is found to be due to the phase volume effect, which originates from the energy and the momentum conservation law. This effect becomes stronger as the removed (knocked out) particle is tightly bound to the target. The tail on the low momentum side of the LMD is enhanced by the momentum shift of the outgoing two nucleons in the interaction region by the attraction of the residue. Such final state interactions distort the scattering waves of the nucleons, thus local momenta of them are different from their asymptotic ones. Therefore, the missing momentum of the knockout reaction in the reaction region differs from the asymptotic one and the momentum distribution of the knockout out nucleon is also distorted. From the above discussions, one may expect that the asymmetry is prominent when the separation energy is large and the beam energy is low, as theoretically predicted in Figs. 6 and 7 of Ref. [33] for (p, pN) and experimentally seen in Figs. 2 and 3 of Ref. [31] and Fig. 3 of Ref. [32] for nucleon removal reaction with a nucleus target.

Based on the abovementioned discussion, $^{14}\text{O}(p, 2p)^{13}\text{N}$ and $^{14}\text{O}(p, pn)^{13}\text{O}$ were measured at ~ 100 MeV at RIBF, RIKEN [34]. The proton separation energy (S_p) and the neutron separation energy (S_n) of ^{14}O are $S_p = 4.2$ MeV and $S_n = 23.2$ MeV, respectively. Due to the large gap in the separation energy, LMDs of the reactions show completely different shapes. As seen in Fig. 3 (a) and (b), LMD of $^{14}\text{O}(p, 2p)^{13}\text{N}$ shows an almost symmetric shape, as it is expected from its small separation energy. In contrast, $^{14}\text{O}(p, pn)^{13}\text{O}$ shows a long tail

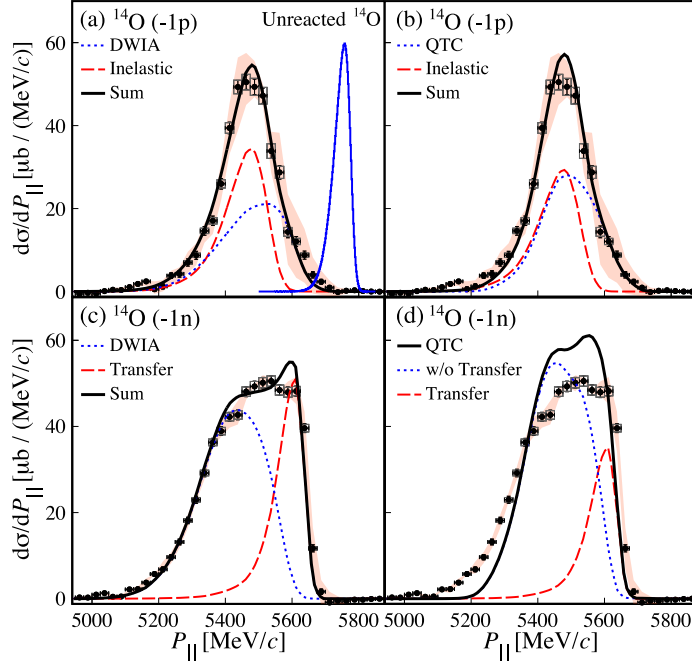


Fig. 3 Longitudinal momentum distributions of $^{14}\text{O}(p, pn)^{13}\text{O}$ and $^{14}\text{O}(p, 2p)^{13}\text{N}$ reactions. Figure is taken from Ref. [34].

in the low momentum side and a sharp cut in the high momentum side due to large S_n as shown in Fig. 3 (c) and (c). Note that a small tail in the low momentum side can be also seen in $^{14}\text{O}(p, 2p)^{13}\text{N}$ LMD due to the small beam energy.

The data were compared with calculations by DWIA and the Quantum Transfer-to-the-Continuum (QTC) calculations [35–38]. In Fig. 3 (a) and (b), the DWIA and QTC results are shown in comparison with the $^{14}\text{O}(p, 2p)^{13}\text{N}$ data, respectively. It was found that a contribution from the inelastic $^{14}\text{O}(p, p')$ reaction followed by one-proton emission (dashed) is nonnegligible and has to be added to the proton knockout cross section (dotted), as shown in Fig. 3 (a) and (b), to reproduce the experimental data. It was also found in Fig. 3 (c) and (d) that the $^{14}\text{O}(p, d)^{13}\text{O}$ transfer component is essential to reproduce the data. It should be noted that the $^{14}\text{O}(p, d)^{13}\text{O}$ cross section (dashed line in Fig. 3 (c)) has to be explicitly

added to the DWIA result (dotted line) since the DWIA framework can only describe the knockout process. On the other hand, both $^{14}\text{O}(p, pn)^{13}\text{O}$ and $^{14}\text{O}(p, d)^{13}\text{O}$ processes can be described in the QTC framework. For comparison with the DWIA result, the QTC result is decomposed into (p, d) and (p, pn) cross sections in Fig. 3 (d).

In Ref. [34], it has been clearly shown that asymmetry also exists in the LMD of the proton-induced knockout reaction, and it strongly depends on the nucleon separation energies. It is also shown that the transfer and the proton decay contribution is negligible at around ~ 100 MeV incident energy. Since such contribution is negligible at higher energy around $250A$ MeV as shown in Fig. 2, it will be interesting to investigate the incident energy dependence of such contributions in the nucleon knockout cross sections.

4 α knockout reaction

The proton induced α knockout reaction, $(p, p\alpha)$, has been utilized to probe the α clustering and its amplitude in a nucleus [5, 6, 39–50]. Recently, thanks to the experimental developments the triple differential cross section of the $(p, p\alpha)$ reaction can be obtained even in the inverse kinematics.

As the first $(p, p\alpha)$ experiment done with MINOS, the four-neutron resonance state was observed by the $^8\text{He}(p, p\alpha)4n$ reaction in the inverse kinematics. The missing mass spectrum of the $4n$ system was reconstructed from the momenta of the charged particles and the energy and the momentum conservation law. The quasi-free α - p scattering close to 180° in the α - p center-of-mass frame was selected in the experiment (See Fig. 4). Choosing such backward angle α - p quasi-free scattering, the α core of ^8He beam is slowed down by a large momentum transfer to the opposite direction of the beam. Thus, the α core is knocked out from ^8He nucleus without disturbing the valence $4n$ system, and they are emitted to forward angle with almost the same velocity as the beam, without almost no transferred momentum.

The missing mass spectrum of the $4n$ system obtained from the $^8\text{He}(p, p\alpha)4n$ reaction is shown in Fig. 5. A clear peak is observed above the threshold as shown in the pink line in Fig. 5. Assuming a Breit-Wigner shaped resonance state, the energy and the width are determined as $2.37 \pm 0.38(\text{stat.}) \pm 0.44(\text{sys.})$ MeV and $1.75 \pm 0.22(\text{stat.}) \pm 0.30(\text{sys.})$ MeV, respectively. Detailed analysis and discussion of the $4n$ resonance state is discussed in other articles of this review.

The triple differential cross section of the $^{10}\text{Be}(p, p\alpha)^6\text{He}$ has been reported on Ref. [13]. The experimental data were compared with theoretical predictions of the DWIA calculations using the Tohsaki-Horiuchi-Schuck-Röpke (THSR) wave function [52–54] and the antisymmetrized molecular dynamics (AMD) framework [55, 56]. Figure 6 shows the comparison

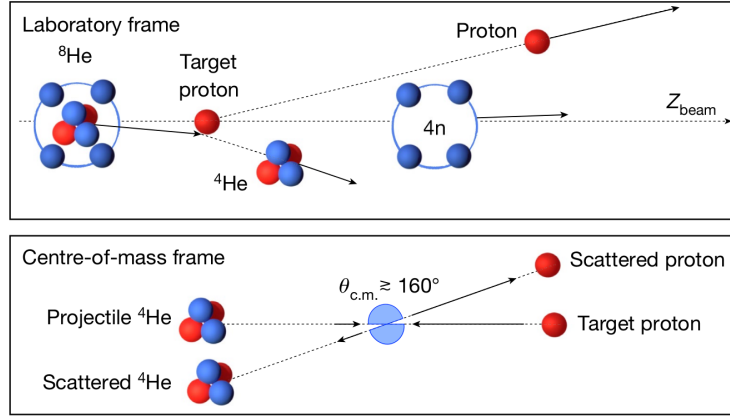


Fig. 4 Schematic illustration of the ${}^8\text{He}(p, p\alpha)4n$ in the inverse kinematics. Top figure: Quasi-free α knockout reaction by the proton target in the laboratory frame. The α core of ${}^8\text{He}$ is knocked out and the valence $4n$ is emitted to the forward direction. Bottom figure: The p - ${}^4\text{He}$ elastic scattering in their center-of-mass frame. The backward angle scattering, $\theta_{c.m.} \gtrsim 160^\circ$, is considered in the experiment. Reprinted figure from [51] Copyright CC BY 4.0.

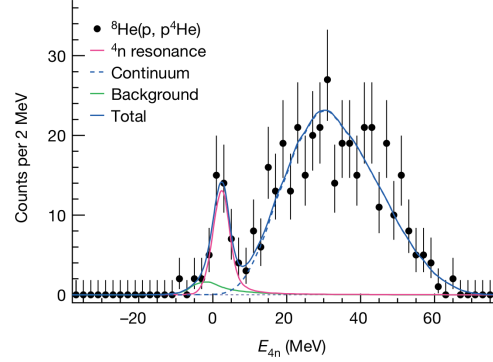


Fig. 5 Observed missing mass spectrum of the $4n$ system in the final state of ${}^8\text{He}(p, p\alpha)4n$ reaction. Reprinted figure from [51] Copyright CC BY 4.0.

between the experimental data and the theoretical results. Both the THSR and AMD amplitudes reproduce the data. Also, as shown in the upper panel of Fig. 6, artificial gas-like and the shell-model-like compact 2α structure of ${}^{10}\text{Be}$ give larger and smaller cross sections, respectively, which indicate upper and lower extreme limits. A similar analysis is ongoing for ${}^{12}\text{Be}(p, p\alpha)8\text{He}$ reaction and the evolution of the 2α structure along the Be isotopes will be revealed by the $(p, p\alpha)$ reactions.

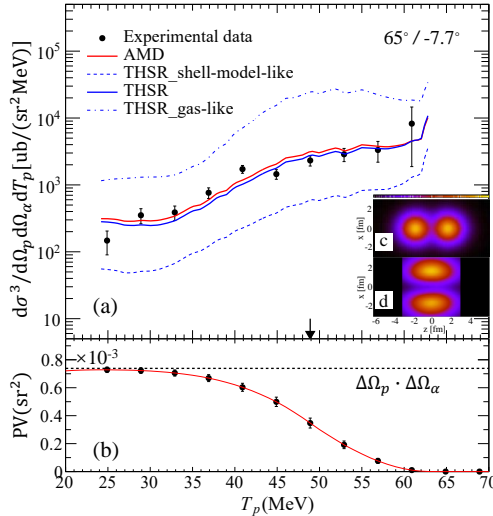


Fig. 6 (a) The triple differential cross section of the $^{10}\text{Be}(p, p\alpha)^6\text{He}$ reaction. The experimental data are shown as a function of the proton emission energy T_p , in comparison with the DWIA calculations using the α amplitudes by THAR and AMD frameworks. (b) The corresponding phase volume of the reaction kinematics. (c) and (d) show the proton and the valence neutron density distributions predicted by THSR, respectively. Reprinted figure with permission from [13] Copyright 2024 by the American Physical Society.

Our interest has been mainly focused on the α clustering in the light-mass region, but recently it has been extended throughout the nuclear chart. Inspired by the theoretical prediction on the α formation on the surface of Sn isotopes [7], α knockout reaction from $^{112,116,120,124}\text{Sn}$ were performed [9]. As shown in Fig. 7 E, $\text{Sn}(p, p\alpha)\text{Cd}$ cross sections and its isotope dependence were obtained, and a theoretical cross section based on the predicted α distribution [7] very well reproduce the isotope dependence. The experiment confirmed the α particle formation on the surface of medium mass nuclei for the first time. Also, the theoretical prediction of the suppression of the α particle formation due to the development of the neutron skin has been verified experimentally.

A capability of α knockout reaction for probing the α formation amplitude (reduced α width) on the surface of α -decay nuclei has been investigated [10]. The idea behind this work is that a large gap in the timescale of the α decay process and the α knockout reaction. For example, a typical α decay nuclei, ^{212}Po in which we may expect $\alpha + ^{208}\text{Pb}$ component, its lifetime is about $0.3 \mu\text{s}$. On the other hand, the time scale of the knockout reaction is in order of approximately $10^{-22} \text{ s} \sim 30 \text{ fm}/c$, which is a typical timescale of direct reactions, which corresponds to the timescale of the incident particle traveling the diameter of a target

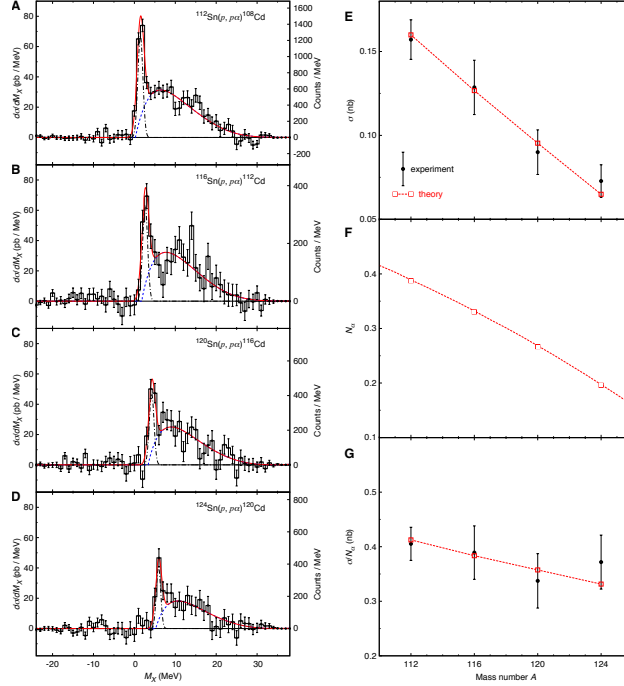


Fig. 7 (A–D) Missing mass spectra of the $(p, p\alpha)$ reaction from ^{112}Sn , ^{116}Sn , ^{120}Sn , ^{124}Sn . (E) Experimental α knockout cross section (black circles with error bars) and theoretical cross sections (red square). (F) Theoretical prediction of the α particle numbers and its isotope dependence [7]. (G) The ratio of the cross section to the α particle number. Reprinted figure with permission from [9] Copyright 2024 by the The American Association for the Advancement of Science.

nucleus. This difference suggests that the α formation probability can be directly observed as α knockout cross section, independently of the α decay process.

The theoretical description of the α formation in heavy nuclei is challenging. Recently, the α -removal strength has been proposed from the mean-field approach [57]. At present, the theory assumes several approximations in order to make the numerical calculations feasible, e.g., the point α approximation. However, as shown in Fig. 4. of Ref. [57], the theory provides not only the α -removal strength leaving the residue in the ground state, but also the strength going to the excited states of the residue. Another new structure theory, a hybrid of the Hartree-Fock and AMD models, has recently been introduced [58]. This model employs a set of localized Gaussians. In contrast to AMD, the number of the localized Gaussians is not limited to the number of nucleons. This overcomes some difficulties in the AMD framework in the heavier mass region, and the binding energy, density distribution, etc. are

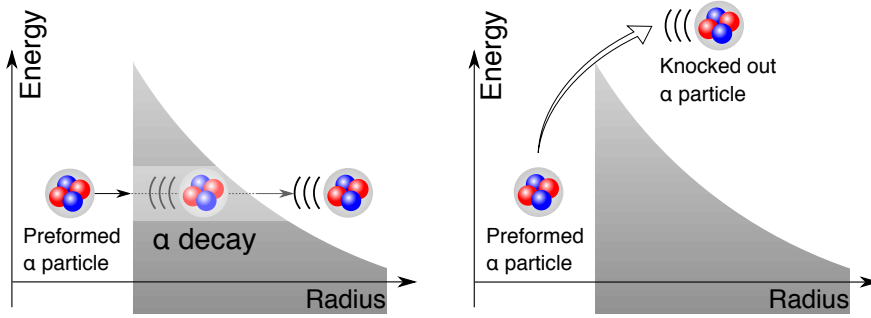


Fig. 8 Illustrations of the α decay process and the α knockout reaction. (left) The α decay is a process in which a preformed α particle penetrates the Coulomb barrier by quantum mechanical effect. (Right) In the α knockout process, a preformed α particle is hit by a high energy beam and knocked out with large energy and momentum transfer. The α particle has enough high energy to go above the Coulomb barrier and is less affected by the barrier.

improved. These developments in the structure theories are essential for future studies of the α formation in the medium-mass nuclei and its systematics.

5 Beyond the standard knockout reaction

As more advanced content, we will introduce two proton knockout reactions and various cluster knockout reactions. Correctly handling the α knockout reaction's surface nature allows the reduced α decay width to be measured via an α particle release mechanism that is less dependent on the Coulomb barrier. Furthermore, applying the surface nature of the α knockout reaction may lead to highly polarized residual nuclei. To quantitatively discuss the number of deuteron clusters formed in deuteron knockout reactions, it is essential to understand the complex reaction mechanism and theoretical progress has been made.

5.1 NN correlation probed by knockout reaction

In Ref. [59], the dineutron correlation in Borromean nuclei ${}^8\text{He}$ and the ${}^8\text{He}(p, pn){}^5\text{He}$ reaction were theoretically investigated, based on the $\alpha + n + n$ three-body model. The theory predicted a large nn correlation angle in the ground state of ${}^6\text{He}$ in the momentum space; thus, it suggested a dineutron correlation in the coordinate space. It was also found that the dineutron correlation is enhanced by looking at the low α - n momentum region around $k_{\alpha-n} = 0.2 \text{ fm}^{-1}$ of ${}^5\text{He}$ residue. In contrast, it was suggested that the cigar-like configuration could be seen in a high α - n momentum region around $k_{\alpha-n} = 1.0 \text{ fm}^{-1}$. It was reported that the resonance state of the ${}^5\text{He}(3/2^-)$ at $k_{\alpha-n} \sim 0.2 \text{ fm}^{-1}$ drastically changes

the relation between the dineutron correlation in ${}^6\text{He}$ and the knockout reaction observable; it is important to choose a suitable knockout reaction kinematics to minimize the effect from the ${}^5\text{He}$ resonance. To avoid the effect from the resonance state, the authors of Ref. [59] suggested to choose off-resonant α - n relative momenta, $k_{\alpha-n} \sim 0.1 \text{ fm}^{-1}$, to see the dineutron correlation by the knockout reaction. The feasibility of the ${}^6\text{He}(p, pn){}^5\text{He}$ reaction using a high-intensity radioactive beam and the MINOS is also discussed in this paper.

Building on the theoretical predictions from Ref. [59], the localized dineutron formation in the ${}^{11}\text{Li}$ nucleus was experimentally confirmed through the kinematically complete ${}^{11}\text{Li}(p, pn){}^{10}\text{Li}$ reaction [60]. This experiment, made possible by a high-intensity ${}^{11}\text{Li}$ beam at RIBF and the MINOS, revealed the quasi-free knockout reaction with a momentum transfer larger than 1.5 fm^{-1} , significantly exceeding the two-neutron momentum in ${}^{11}\text{Li}$. The two-neutron $(1s)^2$, $(0p)^2$, and $(0d)^2$ configurations were effectively separated by selecting the missing momentum and the relative energy. In the missing momentum $k = 0.25\text{--}0.35 \text{ fm}^{-1}$ region, the s - and the p -wave neutron components showed similar magnitude, indicating an enhanced dineutron-like correlation in this region. The mean two-neutron correlation angle $\langle\theta_{nf}\rangle(k) = \int \theta_{nf} P(\cos\theta_{nf}, k) d(\cos\theta_{nf})$, with $P(\cos\theta_{nf}, k)$ being a normalized $\cos\theta_{nf}$ distribution, is a key parameter in understanding dineutron correlation. In Fig. 9 (reprint from Ref. [60] Fig. 4), it is clearly shown that $\langle\theta_{nf}\rangle$ has a clear peak $\langle\theta_{nf}\rangle \sim 100^\circ$ at $k \sim 0.3 \text{ fm}^{-1}$, indicating the presence of dineutron correlation in this region. It is also found

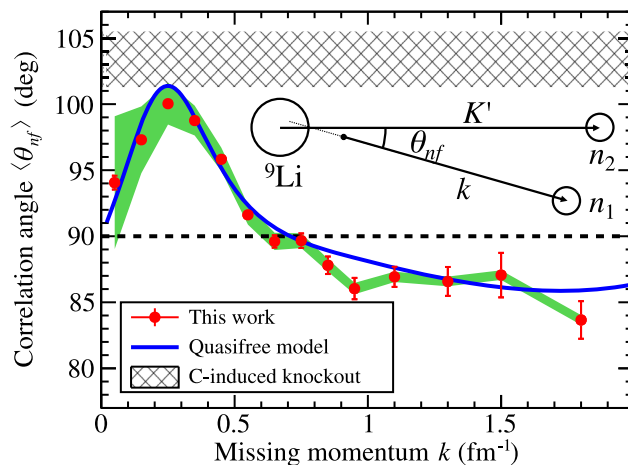


Fig. 9 Mean value of the two-neutron correlation angle $\langle\theta_{nf}\rangle$ in the momentum space. The red points are the experimental data and the blue solid line is the quasi-free model result. Reprinted figure with permission from [60] Copyright 2024 by the American Physical Society.

that $\langle\theta_{nf}\rangle \sim 90^\circ$ at $k \sim 0$, it becomes less than 90° in $k \gtrsim 0.6 \text{ fm}^{-1}$ region. A combination of the ${}^9\text{Li}+n+n$ three-body model and the knockout reaction model of Ref. [59] well reproduces the experimental data as shown in the blue solid line in Fig. 9. This k dependence of $\langle\theta_{nf}\rangle$ is consistent with the theoretical analysis of Ref. [59]. The theoretical model suggests that the peak of $\langle\theta_{pf}\rangle$ at $k \sim 0.3 \text{ fm}^{-1}$ can be interpreted as the dineutron correlation having a peak at $r \sim 3.6 \text{ fm}$ from the center of ${}^9\text{Li}$.

A systematic survey of the inclusive $(p, 2p)$ and (p, pn) cross section from 55 neutron-rich nuclei has been done in Ref. [61]. The measured inclusive $(p, 2p)$ cross sections are shown in Fig. 10 (a). The even- (odd-) Z projectiles are shown as open (filled) circles in Fig. 10 (a).

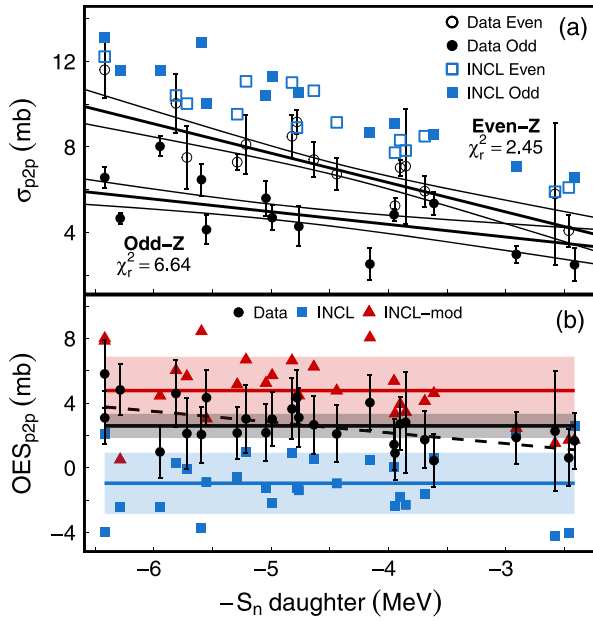


Fig. 10 (a) Comparison between the inclusive $(p, 2p)$ cross section (black circles) and the intranuclear cascade (INCL) calculations (squares) and (b) odd-even splitting of the cross sections, as the neutron separation energy $-S_n$ dependence. See Ref. [61] for details. Reprinted figure with permission from [61] Copyright 2024 by the American Physical Society.

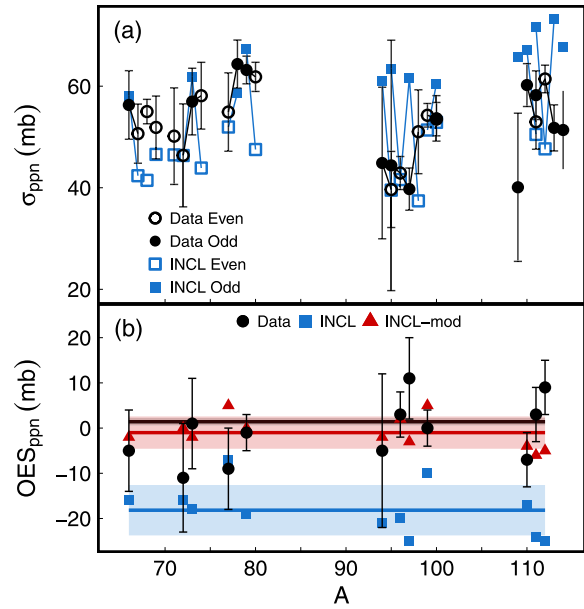


Fig. 11 (a) Comparison between the inclusive (p, pn) cross section (black circles) and the intranuclear cascade (INCL) calculations (squares) and (b) odd-even splitting of the cross sections, as the mass number dependence. See Ref. [61] for details. Reprinted figure with permission from [61] Copyright 2024 by the American Physical Society.

Both the $(p, 2p)$ cross section from the even and odd Z projectile shows a decreasing trend as S_n decreases, but an odd-even effect can be seen; the even- Z projectiles give a larger

cross section than odd- Z projectiles for the same S_n of the residue. The Akaike information criterion (AIC) [62] analysis supports two separate linear trends with different slopes for even and odd Z projectiles. Figure 10 (b) shows the odd-even splitting (OES) of the cross section, OES_{p2p} . See Ref. [61] for the definition of OES. A constant regression (black solid line) and a linear regression with weak S_n dependence (black dashed line) are possible by the χ^2 analysis. The linear decreasing trend of the $(p, 2p)$ cross sections can be explained as follows. As the nucleus becomes neutron-rich nuclei, fewer bound states are below S_n of the $A - 1$ residual nuclei. Therefore, the $(p, 2p)$ cross section decreases as S_n decreases. The OES is related to the pairing interaction. In $(p, 2p)$ reaction on odd- Z nuclei leaving even- Z residue, the pairing interaction reduces the level density. If the weak linear decreasing trend is true, such dependence can be understood by reducing the pairing as the neutron number increases, as suggested by the mass measurement [63] and the predictions [64, 65].

In contrast to the $(p, 2p)$ case, the (p, pn) cross sections do not show S_n dependence as shown in Fig. 11 (a). This is understood as follows. As the neutron number increases along the isotopic chain, the neutron removal cross section is expected to increase. However, as discussed in the $(p, 2p)$ case, the S_n of the residual nuclei decreases with the mass number, and hence the number of the bound states of the residue decreases as the neutron number increases. No odd-even splitting was observed in the (p, pn) case as shown in Fig. 11 (b). This is because the reduced level density in the even- N residues compensates for larger S_n of them. Thus the total (p, pn) cross sections leaving bound residues are similar in even- N and odd- N cases. See Ref. [61] for details and discussions on the comparison with the INCL calculations.

5.2 Knockout reaction of fragile cluster and NN correlation

In contrast to the (p, pN) and $(p, p\alpha)$ reactions, knocking out a fragile particle, e.g., a deuteron is not as simple as (p, pN) and $(p, p\alpha)$. The description of such reactions is theoretically challenging. The deuteron knockout reaction, (p, pd) , will be a probe for the p - n correlation in a nucleus. Since the deuteron is fragile and its breakup and reformation processes play important roles in deuteron-involved reactions, the (p, pd) reaction has to be described with a theory beyond the standard DWIA. Recently, a combination of the DWIA and the continuum-discretized coupled channels method [66–68] has been developed [69]. The framework, CDCCIA, contains two important features. One is the description of the elementary process. CDCCIA employs the NN effective interaction as the transition interaction and the transition between the p - n ground state (deuteron) and the continuum states in the elementary process is taken into account. The other is the CDCC description for the $p+n+B$ three-body wave function in the final state of the (p, pd) reaction. The transition

between the p - n ground and continuum states by the final state interaction is also taken into account by the CDCC manner. These treatments allow us to connect the correlated p - n pair to the (p, pd) and (p, ppn) reaction observables, as illustrated in Fig. 12.

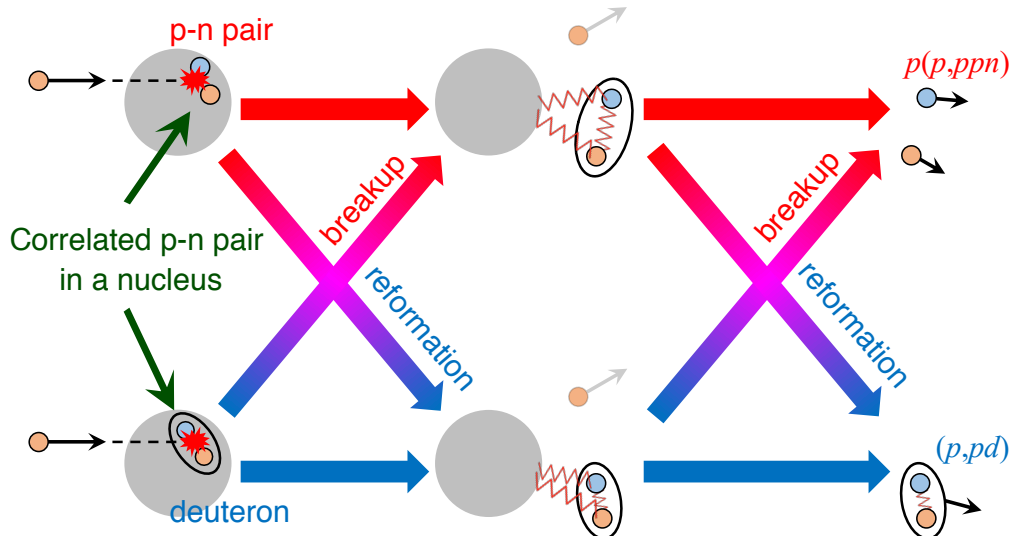


Fig. 12 Possible reaction path of the correlated p - n pair in a nucleus to the p - n pair knockout reaction observables.

Before the bombarded proton hits the p - n pair, the p - n pair is not necessarily the deuteron ground state. The information of the p - n pair in the target nucleus should be given from structure theory predictions, e.g., the two-nucleon amplitude, as an input to the CDCCIA calculation. Once such input is given, the CDCCIA framework can describe the breakup and the reformation processes of the p - n pair, by the elementary process and the final state interaction, as shown in Fig. 12. The CDCCIA framework is not only available for (p, pd) and (p, ppn) but extensible to $(p, 3p)$ and (p, pnn) in a similar manner. Only the difference should be whether the two-nucleon pair has the bound state or not.

5.3 $(p, p2N)$ reaction and multiple scattering

The sequential $(p, p2N)$ reaction is also interesting as well as the pair knockout process. The two-proton knockout reaction, $(p, 3p)$, were measured from neutron-rich nuclei at $\sim 250A$ MeV in inverse kinematics [70]. In this experiment, the angular distribution of the three emitted protons was measured for the first time. Figure 13 shows the angular dependence of the measured $(p, 3p)$ events as a function of the projected angle φ_s , the beam angle θ , and the angle between the scattered protons λ . See Fig. 1 of Ref. [70] for the definition of φ_s , θ and λ . The data were compared with three models: (1) Sequential (2) Pair breakup

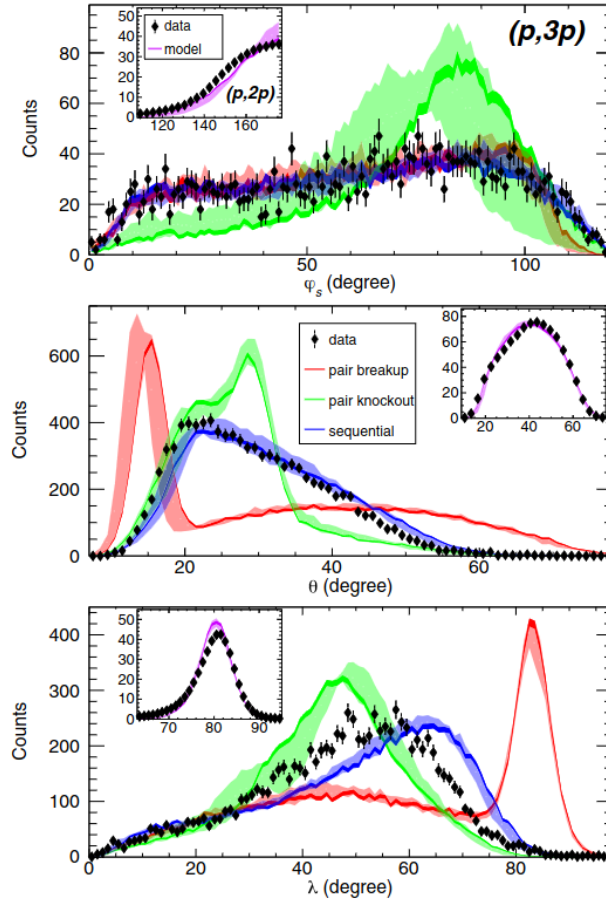


Fig. 13 Angular distributions of $^{81}\text{Ga}(p, 3p)$ reaction. Pair breakup, pair knockout, and sequential model calculations are also shown in red, green, and blue bands, respectively. The figure is taken from Fig. 4 of Ref. [70].

and (3) Pair knockout. (1) Sequential process assumes that independent p - p binary collision occurs twice sequentially. (2) Pair breakup assumes a correlated p - p pair inside the nucleus and the center-of-mass of the pair is at rest in the nucleus rest frame. The target proton only interacts with one proton of the proton pair and the p - p binary collision occurs. The other proton of the pair, which was a spectator, is emitted by its initial momentum, which the proton had in the proton pair. (3) Pair knockout assumes that the center-of-mass of the correlated proton pair is knocked out by the target proton in a similar manner as in the naive (p, pd) reaction. See Ref. [70] for a detailed explanation. As shown in Fig. 13, all the angular distributions support the sequential process dominance, though the λ dependence might suggest a small portion of the pair knockout contribution.

Analyses by more sophisticated reaction theory will give us more insight into the nature of $(p, 3p)$ reaction, as well as (p, ppn) and (p, pnn) . It is also interesting if one can select one process out of three possible mechanisms, sequential, pair breakup, and pair knockout by choosing proper kinematics of the $(p, p2N)$ reaction since populated states and its yield by $(p, p2N)$ reaction should depend on the reaction mechanisms. CDCCIA framework discussed in Sec. 5.2 will be one of the most suitable theories for describing the pair knockout type $(p, 3p)$ process.

6 Summary

SEASTAR project and MINOS have revealed the nucleon orbitals and their revolution in neutron-rich nuclei. The simplicity of the reaction mechanism is one of the greatest advantages in understanding and interpreting the knockout reaction observables and their connection to the nuclear structure. The momentum distribution of the residual nuclei tells us the momentum distribution of the struck nucleon inside the nucleus and its single-particle orbitals. The magnitude of the cross section corresponds to the spectroscopic factor. Beyond the standard (p, pN) reaction at hundreds of MeV, new physics directions have been discussed in this chapter.

The nucleon-nucleon correlation is one of the biggest interest. Recently, a combination of the DWIA and CDCC framework, CDCCIA, has proposed to incorporate the NN correlation properly in the description of the pair knockout type $(p, p2N)$ reactions. At this stage, the CDCCIA framework is only applicable to (p, pd) reaction, but shortly the framework will be extended to (p, ppn) , $(p, 3p)$ and $(p, p2n)$ reactions. The NN correlation inside a nucleus will be directly connected to $(p, p2N)$ observables. All the reaction paths, the breakup and reformation effect of the p - n pair by both the elementary process and by the final-state interaction are included in (p, pd) and (p, ppn) description as shown in Fig. 12. Although the p - p and n - n pair do not have the bound state, the continuum-continuum coupling is taken into account as well as in the p - n pair knockout case. An inclusive description of the pair knockout, pair breakup, and sequential $(p, p2N)$ reactions will be necessary for understanding the $(p, p2N)$ reaction mechanism. It is also important to understand the populated states of the reaction residue by the $(p, p2N)$ reactions.

The $4N$ correlation and the α formation have been of great interest since the beginning of the nuclear physics study. Historically, the α formation has been intensively studied at both ends of the nuclear chart, in light nuclei and the α preformation in the α decay nuclei. Recently, the search for the α formation has been extended to the medium mass nuclei and the α formation is found to be universal throughout the nuclear chart. A systematic

understanding of the α formation in unstable nuclei from light to heavy mass regions will be one of the next scopes of the α formation and the α knockout reaction studies.

References

- [1] Gerhard Jacob and TH. A. J. Maris, *Rev. Mod. Phys.*, **38**, 121–142 (01 1966).
- [2] Gerhard Jacob and TH. A. J. Maris, *Rev. Mod. Phys.*, **45**, 6–21 (01 1973).
- [3] N. S. Chant and P. G. Roos, *Phys. Rev. C*, **15**, 57–68 (01 1977).
- [4] N. S. Chant and P. G. Roos, *Phys. Rev. C*, **27**, 1060–1072 (03 1983).
- [5] T. A. Carey, P. G. Roos, N. S. Chant, A. Nadasen, and H. L. Chen, *Phys. Rev. C*, **23**, 576–579 (01 1981).
- [6] T. A. Carey, P. G. Roos, N. S. Chant, A. Nadasen, and H. L. Chen, *Phys. Rev. C*, **29**, 1273–1288 (04 1984).
- [7] S. Typel, *Phys. Rev. C*, **89**, 064321 (06 2014).
- [8] Kazuki Yoshida, Kosho Minomo, and Kazuyuki Ogata, *Phys. Rev. C*, **94**, 044604 (10 2016).
- [9] Junki Tanaka, Zaihong Yang, Stefan Typel, Satoshi Adachi, Shiwei Bai, Patrik van Beek, Didier Beaumel, Yuki Fujikawa, Jiaying Han, Sebastian Heil, Siwei Huang, Azusa Inoue, Ying Jiang, Marco Knösel, Nobuyuki Kobayashi, Yuki Kubota, Wei Liu, Jianling Lou, Yukie Maeda, Yohei Matsuda, Kenjiro Miki, Shoken Nakamura, Kazuyuki Ogata, Valerii Panin, Heiko Scheit, Fabia Schindler, Philipp Schrock, Dmytro Symochko, Atsushi Tamii, Tomohiro Uesaka, Vadim Wagner, Kazuki Yoshida, Juzo Zenihiro, and Thomas Aumann, *Science*, **371**(6526), 260–264 (2021).
- [10] Kazuki Yoshida and Junki Tanaka, *Phys. Rev. C*, **106**, 014621 (07 2022).
- [11] A. Obertelli, A. Delbart, S. Anvar, L. Audirac, G. Authelet, H. Baba, B. Bruyneel, D. Calvet, F. Château, A. Corsi, P. Doornenbal, J. M. Gheller, A. Giganon, C. Lahonde-Hamdoun, D. Leboeuf, D. Loiseau, A. Mohamed, J. Ph. Mols, H. Otsu, C. Péron, A. Peyaud, E. C. Pollacco, G. Prono, J. Y. Rousse, C. Santamaria, and T Uesaka, *Eur. Phys. J. A*, **50**, 8 (2014).
- [12] Tomohiro Uesaka, *Prog. Theor. Exp. Phys.*, page ptae013 (01 2024).
- [13] P. J. Li, D. Beaumel, J. Lee, M. Assié, S. Chen, S. Franchoo, J. Gibelin, F. Hammache, T. Harada, Y. Kanada-En'yo, Y. Kubota, S. Leblond, P. F. Liang, T. Lokotko, M. Lyu, F. M. Marqués, Y. Matsuda, K. Ogata, H. Otsu, E. Rindel, L. Stuhl, D. Suzuki, Y. Togano, T. Tomai, X. X. Xu, K. Yoshida, J. Zenihiro, N. L. Achouri, T. Aumann, H. Baba, G. Cardella, S. Ceruti, A. I. Stefanescu, A. Corsi, A. Frotscher, J. Gao, A. Gillibert, K. Inaba, T. Isobe, T. Kawabata, N. Kitamura, T. Kobayashi, Y. Kondo, A. Kurihara, H. N. Liu, H. Miki, T. Nakamura, A. Obertelli, N. A. Orr, V. Panin, M. Sasano, T. Shimada, Y. L. Sun, J. Tanaka, L. Trache, D. Tudor, T. Uesaka, H. Wang, H. Yamada, Z. H. Yang, and M. Yasuda, *Phys. Rev. Lett.*, **131**, 212501 (11 2023).
- [14] Kazuyuki Ogata, Kazuki Yoshida, and Yoshiki Chazono, *Comput. Phys. Commun.*, **297**, 109058 (2024).
- [15] A.S. Goldhaber, *Physics Letters B*, **53**(4), 306–308 (1974).
- [16] N. Metropolis, R. Bivins, M. Storm, Anthony Turkevich, J. M. Miller, and G. Friedlander, *Phys. Rev.*, **110**, 185–203 (04 1958).
- [17] N. Metropolis, R. Bivins, M. Storm, J. M. Miller, G. Friedlander, and Anthony Turkevich, *Phys. Rev.*, **110**, 204–219 (04 1958).
- [18] Hugo W. Bertini, *Phys. Rev.*, **131**, 1801–1821 (08 1963).
- [19] K. Chen, Z. Fraenkel, G. Friedlander, J. R. Grover, J. M. Miller, and Y. Shimamoto, *Phys. Rev.*, **166**, 949–967 (02 1968).
- [20] Y. Yariv and Z. Fraenkel, *Phys. Rev. C*, **20**, 2227–2243 (12 1979).
- [21] T. Kodama, S. B. Duarte, K. C. Chung, and R. A. M. S. Nazareth, *Phys. Rev. Lett.*, **49**, 536–539 (08 1982).
- [22] Jose Luis Rodríguez-Sánchez, Jean-Christophe David, Davide Mancusi, Alain Boudard, Joseph Cugnon, and Sylvie Leray, *Phys. Rev. C*, **96**, 054602 (11 2017).
- [23] Kenneth M. Watson, *Phys. Rev.*, **89**, 575–587 (02 1953).
- [24] N. C. Francis and K. M. Watson, *Phys. Rev.*, **92**, 291–303 (10 1953).
- [25] W. B. Riesenfeld and K. M. Watson, *Phys. Rev.*, **102**, 1157–1163 (05 1956).
- [26] A.K Kerman, H McManus, and R.M Thaler, *Annals of Physics*, **8**(4), 551–635 (1959).
- [27] T. Wakasa, K. Ogata, and T. Noro, *Prog. Part. Nucl. Phys.*, **96**, 32 (2017).
- [28] S. Chen, J. Lee, P. Doornenbal, A. Obertelli, C. Barbieri, Y. Chazono, P. Navrátil, K. Ogata, T. Otsuka, F. Raimondi, V. Somà, Y. Utsuno, K. Yoshida, H. Baba, F. Browne, D. Calvet, F. Château, N. Chiga, A. Corsi, M. L. Cortés, A. Delbart, J.-M. Gheller, A. Giganon, A. Gillibert, C. Hilaire, T. Isobe, J. Kahlbow, T. Kobayashi, Y. Kubota, V. Lapoux, H. N. Liu, T. Motobayashi, I. Murray, H. Otsu, V. Panin, N. Paul, W. Rodriguez, H. Sakurai, M. Sasano, D. Steppenbeck, L. Stuhl, Y. L. Sun, Y. Togano, T. Uesaka, K. Wimmer, K. Yoneda, N. Achouri, O. Aktas, T. Aumann, L. X. Chung, F. Flavigny, S. Franchoo, I. Gašparić, R.-B. Gerst, J. Gibelin, K. I. Hahn, D. Kim, T. Koizumi, Y. Kondo, P. Koseoglou, C. Lehr, B. D. Linh, T. Lokotko, M. MacCormick, K. Moschner, T. Nakamura, S. Y. Park, D. Rossi, E. Sahin, D. Sohler, P.-A. Söderström, S. Takeuchi, H. Törnqvist, V. Vaquero, V. Wagner, S. Wang, V. Werner, X. Xu, H. Yamada, D. Yan, Z. Yang, M. Yasuda, and L. Zanetti, *Phys. Rev. Lett.*, **123**, 142501 (09 2019).

- [29] Takaharu Otsuka, Rintaro Fujimoto, Yutaka Utsuno, B. Alex Brown, Michio Honma, and Takahiro Mizusaki, *Phys. Rev. Lett.*, **87**, 082502 (08 2001).
- [30] Takaharu Otsuka, Toshio Suzuki, Rintaro Fujimoto, Hubert Grawe, and Yoshinori Akaishi, *Phys. Rev. Lett.*, **95**, 232502 (11 2005).
- [31] A. Gade, D. Bazin, C. A. Bertulani, B. A. Brown, C. M. Campbell, J. A. Church, D. C. Dinca, J. Enders, T. Glasmacher, P. G. Hansen, Z. Hu, K. W. Kemper, W. F. Mueller, H. Olliver, B. C. Perry, L. A. Riley, B. T. Roeder, B. M. Sherrill, J. R. Terry, J. A. Tostevin, and K. L. Yurkewicz, *Phys. Rev. C*, **71**, 051301 (05 2005).
- [32] T. Nakamura, N. Kobayashi, Y. Kondo, Y. Satou, J. A. Tostevin, Y. Utsuno, N. Aoi, H. Baba, N. Fukuda, J. Gibelin, N. Inabe, M. Ishihara, D. Kameda, T. Kubo, T. Motobayashi, T. Ohnishi, N. A. Orr, H. Otsu, T. Otsuka, H. Sakurai, T. Sumikama, H. Takeda, E. Takeshita, M. Takechi, S. Takeuchi, Y. Togano, and K. Yoneda, *Phys. Rev. Lett.*, **112**, 142501 (04 2014).
- [33] Kazuyuki Ogata, Kazuki Yoshida, and Kosho Minomo, *Phys. Rev. C*, **92**, 034616 (09 2015).
- [34] T. Pohl, Y. L. Sun, A. Obertelli, J. Lee, M. Gómez-Ramos, K. Ogata, K. Yoshida, B. S. Cai, C. X. Yuan, B. A. Brown, H. Baba, D. Beaumel, A. Corsi, J. Gao, J. Gibelin, A. Gillibert, K. I. Hahn, T. Isobe, D. Kim, Y. Kondo, T. Kobayashi, Y. Kubota, P. Li, P. Liang, H. N. Liu, J. Liu, T. Lokotko, F. M. Marqués, Y. Matsuda, T. Motobayashi, T. Nakamura, N. A. Orr, H. Otsu, V. Panin, S. Y. Park, S. Sakaguchi, M. Sasano, H. Sato, H. Sakurai, Y. Shimizu, A. I. Stefanescu, L. Stuhl, D. Suzuki, Y. Togano, D. Tudor, T. Uesaka, H. Wang, X. Xu, Z. H. Yang, K. Yoneda, and J. Zenihiro, *Phys. Rev. Lett.*, **130**, 172501 (04 2023).
- [35] A. M. Moro, *Phys. Rev. C*, **92**, 044605 (10 2015).
- [36] M. Gómez-Ramos, J. Casal, and A.M. Moro, *Phys. Lett. B*, **772**, 115–120 (2017).
- [37] M. Gómez-Ramos and A.M. Moro, *Physics Letters B*, **785**, 511–516 (2018).
- [38] M. Gómez-Ramos, A. Deltuva, and A. M. Moro, *Phys. Rev. C*, **102**, 064613 (12 2020).
- [39] B. Gottschalk and S. L. Kannenberg, *Phys. Rev. C*, **2**, 24–40 (07 1970).
- [40] D. Bachelier, M. Bernas, O. M. Bilaniuk, J. L. Boyard, J. C. Jourdain, and P. Radvanyi, *Phys. Rev. C*, **7**, 165–169 (01 1973).
- [41] D. Bachelier, J.L. Boyard, T. Hennino, H.D. Holmgren, J.C. Jourdain, P. Radvanyi, P.G. Roos, and M. Roy-Stephan, *Nucl. Phys. A*, **268**(3), 488–512 (1976).
- [42] P. G. Roos, N. S. Chant, A. A. Cowley, D. A. Goldberg, H. D. Holmgren, and R. Woody, *Phys. Rev. C*, **15**, 69–83 (01 1977).
- [43] G. Landaud, A. Devaux, P. Delpierre, J. Kahane, R. Sené, J. Yonnet, and R. Anne, *Phys. Rev. C*, **18**, 1776–1780 (10 1978).
- [44] A. Nadasen, N. S. Chant, P. G. Roos, T. A. Carey, R. Cowen, C. Samanta, and J. Wesick, *Phys. Rev. C*, **22**, 1394–1400 (10 1980).
- [45] C. W. Wang, P. G. Roos, N. S. Chant, G. Ciangaru, F. Khazaie, D. J. Mack, A. Nadasen, S. J. Mills, R. E. Warner, E. Norbeck, F. D. Becchetti, J. W. Janecke, and P. M. Lister, *Phys. Rev. C*, **31**, 1662–1672 (05 1985).
- [46] A. Nadasen, P. G. Roos, N. S. Chant, C. C. Chang, G. Ciangaru, H. F. Breuer, J. Wesick, and E. Norbeck, *Phys. Rev. C*, **40**, 1130–1135 (09 1989).
- [47] T. Yoshimura, A. Okihana, R.E. Warner, N.S. Chant, P.G. Roos, C. Samanta, S. Kakigi, N. Koori, M. Fujiwara, N. Matsuoka, K. Tamura, E. Kubo, and K. Ushiro, *Nucl. Phys. A*, **641**(1), 3–20 (1998).
- [48] R. Neveling, A. A. Cowley, Z. Buthelezi, S. V. Försch, H. Fujita, G. C. Hillhouse, J. J. Lawrie, G. F. Steyn, F. D. Smit, S. M. Wyngaardt, N. T. Botha, L. Mudau, and S. S. Ntshangase, *Phys. Rev. C*, **77**, 037601 (03 2008).
- [49] A. A. Cowley, J. Mabiala, E. Z. Buthelezi, S. V. Försch, R. Neveling, F. D. Smit, G. F. Steyn, and J. J. van Zyl, *Europhysics Letters*, **85**(2), 22001 (01 2009).
- [50] J. Mabiala, A. A. Cowley, S. V. Försch, E. Z. Buthelezi, R. Neveling, F. D. Smit, G. F. Steyn, and J. J. Van Zyl, *Phys. Rev. C*, **79**, 054612 (05 2009).
- [51] M. Duer, T. Aumann, R. Gernhäuser, V. Panin, S. Paschalis, D. M. Rossi, N. L. Achouri, D. Ahn, H. Baba, C. A. Bertulani, M. Böhmer, K. Boretzky, C. Caesar, N. Chiga, A. Corsi, D. Cortina-Gil, C. A. Douma, F. Dufter, Z. Elekes, J. Feng, B. Fernández-Domínguez, U. Forsberg, N. Fukuda, I. Gasparic, Z. Ge, J. M. Gheller, J. Gibelin, A. Gillibert, K. I. Hahn, Z. Halász, M. N. Harakeh, A. Hirayama, M. Holl, N. Inabe, T. Isobe, J. Kahlbow, N. Kalantar-Nayestanaki, D. Kim, S. Kim, T. Kobayashi, Y. Kondo, D. Körper, P. Koseoglou, Y. Kubota, I. Kuti, P. J. Li, C. Lehr, S. Lindberg, Y. Liu, F. M. Marqués, S. Masuoka, M. Matsumoto, J. Mayer, K. Miki, B. Monteagudo, T. Nakamura, T. Nilsson, A. Obertelli, N. A. Orr, H. Otsu, S. Y. Park, M. Parlog, P. M. Potlog, S. Reichert, A. Revel, A. T. Saito, M. Sasano, H. Scheit, F. Schindler, S. Shimoura, H. Simon, L. Stuhl, H. Suzuki, D. Symochko, H. Takeda, J. Tanaka, Y. Togano, T. Tomai, H. T. Törnqvist, J. Tscheuschner, T. Uesaka, V. Wagner, H. Yamada, B. Yang, L. Yang, Z. H. Yang, M. Yasuda, K. Yoneda, L. Zanetti, J. Zenihiro, and M. V. Zhukov, *Nature*, **606**(7915), 678–682 (06 2022).
- [52] A. Tohsaki, H. Horiuchi, P. Schuck, and G. Röpke, *Phys. Rev. Lett.*, **87**, 192501 (10 2001).

- [53] Mengjiao Lyu, Zhongzhou Ren, Bo Zhou, Yasuro Funaki, Hisashi Horiuchi, Gerd Röpke, Peter Schuck, Akihiro Tohsaki, Chang Xu, and Taichi Yamada, *Phys. Rev. C*, **93**, 054308 (05 2016).
- [54] Mengjiao Lyu, Kazuki Yoshida, Yoshiko Kanada-En'yo, and Kazuyuki Ogata, *Phys. Rev. C*, **97**, 044612 (04 2018).
- [55] Yoshiko Kanada-En'yo, *Phys. Rev. C*, **91**, 014315 (01 2015).
- [56] Yoshiko Kanada-En'yo, *Phys. Rev. C*, **93**, 024322 (02 2016).
- [57] Takashi Nakatsukasa and Nobuo Hinohara, *Phys. Rev. C*, **108**, 014318 (07 2023).
- [58] Masaaki Kimura and Yasutaka Taniguchi, *Progress of Theoretical and Experimental Physics*, **2024**(9), 093D01 (08 2024).
- [59] Yuma Kikuchi, Kazuyuki Ogata, Yuki Kubota, Masaki Sasano, and Tomohiro Uesaka, *Progress of Theoretical and Experimental Physics*, **2016**(10), 103D03 (10 2016).
- [60] Y. Kubota, A. Corsi, G. Authelet, H. Baba, C. Caesar, D. Calvet, A. Delbart, M. Dozono, J. Feng, F. Flavigny, J.-M. Gheller, J. Gibelin, A. Giganon, A. Gillibert, K. Hasegawa, T. Isobe, Y. Kanaya, S. Kawakami, D. Kim, Y. Kikuchi, Y. Kiyokawa, M. Kobayashi, N. Kobayashi, T. Kobayashi, Y. Kondo, Z. Korkulu, S. Koyama, V. Lapoux, Y. Maeda, F. M. Marqués, T. Motobayashi, T. Miyazaki, T. Nakamura, N. Nakatsuka, Y. Nishio, A. Obertelli, K. Ogata, A. Ohkura, N. A. Orr, S. Ota, H. Otsu, T. Ozaki, V. Panin, S. Paschalis, E. C. Pollacco, S. Reichert, J.-Y. Roussé, A. T. Saito, S. Sakaguchi, M. Sako, C. Santamaria, M. Sasano, H. Sato, M. Shikata, Y. Shimizu, Y. Shindo, L. Stuhl, T. Sumikama, Y. L. Sun, M. Tabata, Y. Togano, J. Tsubota, Z. H. Yang, J. Yasuda, K. Yoneda, J. Zenihiro, and T. Uesaka, *Phys. Rev. Lett.*, **125**(25), 252501–1–252501–7 (12 2020).
- [61] N. Paul, A. Obertelli, C. A. Bertulani, A. Corsi, P. Doornenbal, J. L. Rodriguez-Sanchez, G. Authelet, H. Baba, D. Calvet, F. Château, S. Chen, A. Delbart, J.-M. Gheller, A. Giganon, A. Gillibert, T. Isobe, V. Lapoux, M. Matsushita, S. Momiyama, T. Motobayashi, M. Niikura, H. Otsu, C. Péron, A. Peyaud, E. C. Pollacco, J.-Y. Roussé, H. Sakurai, C. Santamaria, M. Sasano, Y. Shiga, D. Steppenbeck, S. Takeuchi, R. Taniuchi, T. Uesaka, H. Wang, K. Yoneda, T. Ando, T. Arici, A. Blazhev, F. Browne, A. M. Bruce, R. Carroll, L. X. Chung, M. L. Cortés, M. Dewald, B. Ding, Zs. Dombradi, F. Flavigny, S. Franchoo, F. Giacoppo, M. Górska, A. Gottardo, K. Hadynska-Klek, Z. Korkulu, S. Koyama, Y. Kubota, A. Jungclaus, J. Lee, M. Lettmann, B. D. Linh, J. Liu, Z. Liu, C. Lizarazo, C. Louchart, R. Lozeva, K. Matsui, T. Miyazaki, K. Moschner, S. Nagamine, N. Nakatsuka, C. Nita, S. Nishimura, C. R. Nobs, L. Olivier, S. Ota, Z. Patel, Zs. Podolyák, M. Rudigier, E. Sahin, T. Y. Saito, C. Shand, P.-A. Söderström, I. G. Stefan, T. Sumikama, D. Suzuki, R. Orlandi, V. Vaquero, Zs. Vajta, V. Werner, K. Wimmer, J. Wu, and Z. Xu, *Phys. Rev. Lett.*, **122**, 162503 (04 2019).
- [62] H. Akaike, *IEEE Transactions on Automatic Control*, **19**(6), 716–723 (1974).
- [63] X. L. Tu, X. G. Zhou, D. J. Vieira, J. M. Wouters, Z. Y. Zhou, H. L. Seifert, and V. G. Lind, *Zeitschrift für Physik A Atomic Nuclei*, **337**(4), 361–366 (12 1990).
- [64] David G. Madland and J. Rayford Nix, *Nuclear Physics A*, **476**(1), 1–38 (1988).
- [65] A. Pastore, J. Margueron, P. Schuck, and X. Viñas, *Phys. Rev. C*, **88**, 034314 (09 2013).
- [66] Masayasu Kamimura, Masanobu Yahiro, Yasunori Iseri, Yukinori Sakuragi, Hirofumi Kameyama, and Mitsuji Kawai, *Prog. Theor. Phys. Suppl.*, **89**, 1–10 (1986).
- [67] N. Austern, Y. Iseri, M. Kamimura, M. Kawai, G. Rawitscher, and M. Yahiro, *Physics Reports*, **154**(3), 125–204 (1987).
- [68] Masanobu Yahiro, Kazuyuki Ogata, Takuma Matsumoto, and Kosho Minomo, *Prog. Theor. Exp. Phys.*, **2012**(1), 01A206 (2012).
- [69] Yoshiki Chazono, Kazuki Yoshida, and Kazuyuki Ogata, *Phys. Rev. C*, **106**, 064613 (12 2022).
- [70] A. Frotscher, M. Gómez-Ramos, A. Obertelli, P. Doornenbal, G. Authelet, H. Baba, D. Calvet, F. Château, S. Chen, A. Corsi, A. Delbart, J.-M. Gheller, A. Giganon, A. Gillibert, T. Isobe, V. Lapoux, M. Matsushita, S. Momiyama, T. Motobayashi, M. Niikura, H. Otsu, N. Paul, C. Péron, A. Peyaud, E. C. Pollacco, J.-Y. Roussé, H. Sakurai, C. Santamaria, M. Sasano, Y. Shiga, N. Shimizu, D. Steppenbeck, S. Takeuchi, R. Taniuchi, T. Uesaka, H. Wang, K. Yoneda, T. Ando, T. Arici, A. Blazhev, F. Browne, A. M. Bruce, R. Carroll, L. X. Chung, M. L. Cortés, M. Dewald, B. Ding, Zs. Dombradi, F. Flavigny, S. Franchoo, F. Giacoppo, M. Górska, A. Gottardo, K. Hadynska-Klek, Z. Korkulu, S. Koyama, Y. Kubota, A. Jungclaus, J. Lee, M. Lettmann, B. D. Linh, J. Liu, Z. Liu, C. Lizarazo, C. Louchart, R. Lozeva, K. Matsui, T. Miyazaki, K. Moschner, S. Nagamine, N. Nakatsuka, C. Nita, S. Nishimura, C. R. Nobs, L. Olivier, S. Ota, Z. Patel, Zs. Podolyák, M. Rudigier, E. Sahin, T. Y. Saito, C. Shand, P.-A. Söderström, I. G. Stefan, T. Sumikama, D. Suzuki, R. Orlandi, V. Vaquero, Zs. Vajta, V. Werner, K. Wimmer, J. Wu, and Z. Xu, *Phys. Rev. Lett.*, **125**, 012501 (06 2020).